Journal of Medicinal Chemistry

Article

pubs.acs.org/jmc

^{125}I-Radiolabeled Morpholine-Containing Arginine–Glycine–Aspartate (RGD) Ligand of $\alpha_v\beta_3$ Integrin As a Molecular Imaging Probe for Angiogenesis

Francesca Bianchini,[†,‡] Nicoletta Cini,[§] Andrea Trabocchi,[∥,#] Anna Bottoncetti,[§] Silvia Raspanti,[#] Eleonora Vanzi,[#,#] Gloria Menchi,[∥,#] Antonio Guarna,*[,∥,#] Alberto Pupi,*[,#,#,‡] and Lido Calorini*[,†,‡]

[†]Department of Experimental Pathology and Oncology, University of Florence, Viale Morgagni 50, 50134 Florence, Italy

[‡]Istituto Toscano Tumori (ITT), Via T. Alderotti 26N, 50139 Florence, Italy

[§]Azienda Ospedaliera Universitaria Careggi (AOUC), Largo Brambilla 3, 50134 Florence, Italy

[∥]Department of Chemistry "Ugo Schiff", University of Florence, Via della Lastruccia 13, 50019 Sesto Fiorentino, Florence, Italy

[#]Interdepartmental Center for Preclinical Development of Molecular Imaging (CISPIM), University of Florence, Viale Morgagni 85, 50134 Florence, Italy

[#]Department of Clinical Physiopathology, Nuclear Medicine Unit, University of Florence, Viale Morgagni 85, 50134 Florence

Supporting Information

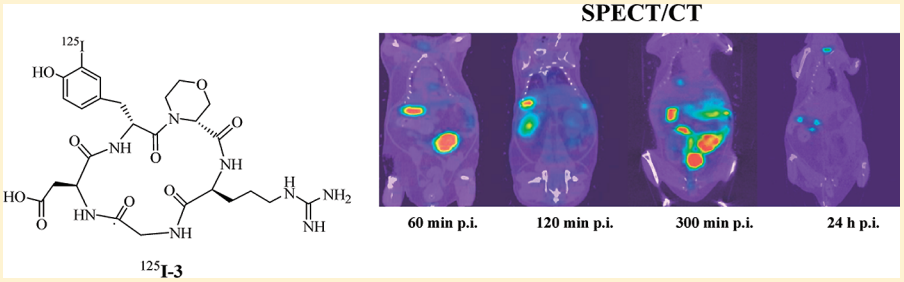

ABSTRACT: In this paper, using a hybrid small-animal Micro SPECT/CT imaging system, we report that a new ^{125}I-Cilengitide-like RGD-cyclopentapeptide, containing D-morpholine-3-carboxylic acid, interacts in vivo with $\alpha_v\beta_3$ integrin expressed by melanoma cells. Images clearly show that the ^{125}I-compound has the capacity to monitor the growth of a melanoma xenograft. Indeed, retention of the labeled ligand in the tumor mass has a good tumor/background ratio, and a significant reduction of its uptake was observed after injection of unlabeled ligand. These results suggest that the use of ^{125}I-labeled morpholine-based RGD-cyclopentapeptides targeting $\alpha_v\beta_3$ positive tumors may play a role in future therapeutic strategies.

INTRODUCTION

As pointed out by the Food and Drug Agency,[1] a major problem with the health system of western societies is the slowness of drug development. This is because of the increasing cost of new drug pipelines which at present exceeds 1.5 billion dollars.[2] Use of biomarkers as molecular imaging tools in early nonclinical and clinical development provides a more informed scientific basis for the design of pivotal trials and has been already proven useful in simplifying the development of target therapies.[3] Indeed, the method implemented in preclinical phases of drug development by molecular imaging can be translated into clinical trials. In addition, using biomarkers in molecular imaging of small-animal models has become a new important scientific field because the animals can be sequentially used but not sacrificed. At the same time, new molecular imaging technology is extending the sensitivity for defining treatment strategies. Among these strategies, new tumor therapies include Cilengitide, a RGD (arginine–glycine–aspartic acid) mimetic integrin inhibitor with anti-angiogenic property, which is under investigation in phase II[4] and III[5] for the treatment of glioblastoma.

Integrins are heterodimeric glycoprotein transmembrane receptors consisting of various combinations of α and β subunits. These receptors regulate biological processes such as apoptosis, cell adhesion and migration, cell differentiation and angiogenesis, and are key points to determine invasiveness and metastatic dissemination of tumor cells.[6]

Integrins on the surface of tumor cells are quite specific and dictate tumor progression. High expression of integrins characterizes various malignant tumors, such as breast and prostate tumors, ovarian carcinoma, glioblastoma, and malignant melanoma. During the transition from a benign melanocytic lesion to a metastatic malignant melanoma, melanocytes undergo a series of changes in the expression of cell-surface integrins. Among these integrins, the vitronectin

Received: November 30, 2011
Published: May 23, 2012

   dx.doi.org/10.1021/jm2016232 | J. Med. Chem. 2012, 55, 5024–5033

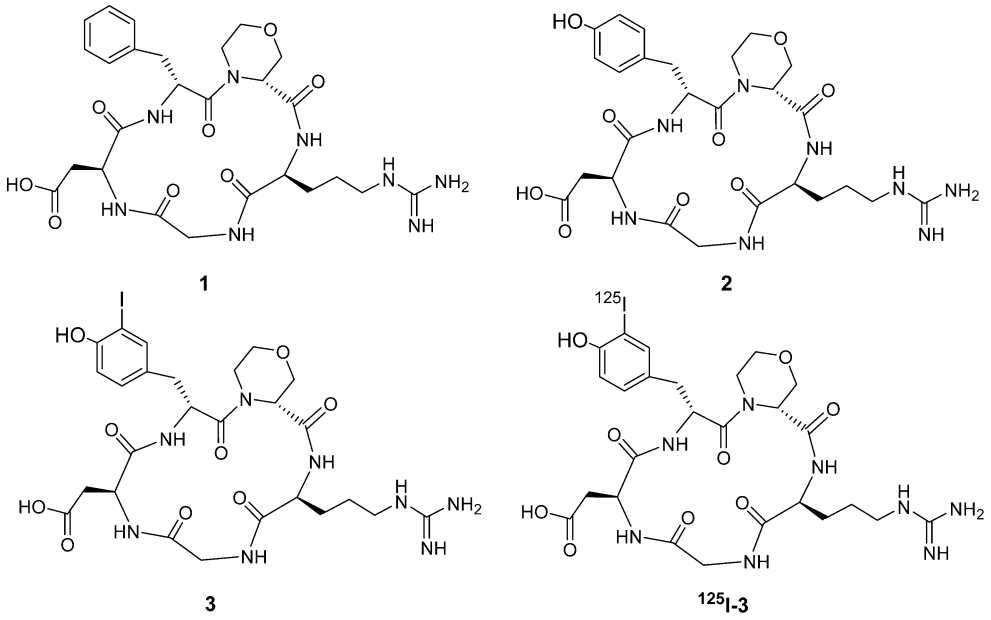

Figure 1. Morpholine-based RGD-cyclopeptides: D-Mor-containing compound **1**, D-Mor-D-Tyr-containing compound **2**, ^{127}I-D-Mor-D-Tyr-containing compound **3**, ^{125}I-D-Mor-D-Tyr-containing compound ^{125}I-**3**.

receptor $\alpha_v\beta_3$ plays a fundamental role in melanoma growth and dissemination. $\alpha_v\beta_3$ integrin overexpression is associated with transition of melanoma cells from the radial to vertical growth phase and characterizes cells at the invasive front of a tumor.[7] In particular, $\alpha_v\beta_3$ integrin favors the localization of MMP-2 on the surface of invasive tumor cells,[8] and it has been demonstrated that the expression of membrane type-1 MMP on the cell surface requires $\alpha_v\beta_3$ integrin.[9] A recent analysis of the gene-expression profile of 34 vertical growth phase of human melanoma indicates that proteins of epithelial-mesenchymal transition (EMT) program, namely $\alpha_v\beta_3$ integrin and MMP-2, are significantly correlated with the metastatic disease.[10]

It is noteworthy that the expression of $\alpha_v\beta_3$ integrin is also characteristic of endothelial cells of tumor vasculature and participates in tumor angiogenesis. Recently, together with $\alpha_v\beta_3$ integrin, an additional RGD integrin, the fibronectin receptor $\alpha_5\beta_1$, which plays a role in tumor angiogenesis, has been found.[11]

The relevance of RGD-dependent integrins in tumor progression has stimulated the search of RGD mimetics to target growth and dissemination of cancer cells and to inhibit tumor angiogenesis.[12]

The interaction between natural ligands and the RGD recognition site of integrins can be inhibited by antagonists that contain the RGD sequence. Inhibition of different RGD-integrins can be modulated by the sequence and the structure of antagonists containing or mimicking the RGD sequence. Recently, many efforts have been dedicated in developing PET[13] and SPECT[14] radiopharmaceuticals addressing the RGD moiety.

Regarding radionuclides for molecular imaging, ^{125}I is gaining interest as a suitable SPECT agent because it is a readily available radionuclide with a half-life of 60.2 days and emission energy in the range of 27−35 KeV. ^{125}I-labeled tracers are commonly used in molecular biology, and many ^{125}I-labeled radiopharmaceuticals are commercially available. In addition, several ^{125}I-labeled imaging probes can be prepared with the aid of commercially available iodination reagents. Molecules labeled with iodine represent a convenient tool for animal models up to humans because substitution of ^{125}I with ^{123}I (159-KeV γ rays with half-life 13.2 h) provides a probe with a path-length suitable for imaging in humans. Furthermore, molecular imaging of iodine-labeled compounds by PET can be accomplished with the positron emitter ^{124}I, and the translation to radionuclide therapy using ^{131}I (emitting β- and γ-rays) can be easily assessed. High-resolution SPECT systems for in vivo imaging of ^{125}I-labeled biomolecules are important for developing new imaging probes for diagnostic and therapeutic approaches.

RESULTS

We recently synthesized and tested a RGD-based cyclopentapeptide containing D-morpholine-3-carboxylic acid (Mor) as a replacement for *N*-methyl-valine as found in Cilengitide (Figure 1, compound **1**). This compound expressed high binding capacity for $\alpha_v\beta_3/\alpha_v\beta_5$ integrins.[15] In this work, we have modified compound **1** by replacing a D-Phe with a D-Tyr (compound **2**) and introducing an iodine atom on the aromatic ring of D-Tyr (compound **3**) with the aim of assessing whether the modified Cilengitide-like inhibitor **3** could be suitable for SPECT imaging using ^{125}I as the radionuclide. We have also demonstrated that the morpholine-based RGD-cyclopentapeptides **1**−**3** interact with $\alpha_v\beta_3$ integrin in vitro and in vivo, and that the ^{125}I-labeled compound ^{125}I-**3** may be used to monitor melanoma xenografts with a hybrid small-animal Micro SPECT/CT imaging system.

Synthesis. Compound **2** was prepared as previously reported[15] with direct labeling with NaI (1:1 molar ratio) using chloramine-T as the oxidizing reagent in phosphate buffered saline solution (PBS). The reaction was quenched with sodium metabisulfite, and the crude product was purified by semipreparative HPLC to give compound **3** (4.7 mg, 32%). Compound ^{125}I-**3** was prepared starting from compound **2** and Na^{125}I (18:1 molar ratio) (as for compound **3**). The crude reaction mixture was purified by preparative HPLC, and the

dx.doi.org/10.1021/jm2016232 | J. Med. Chem. 2012, 55, 5024−5033

radioactivity was monitored with a γ-counter (see Figure S1, Supporting Information). The radiolabeling procedure to obtain ^{125}I-**3** resulted in a clean iodination reaction with a radiochemical yield of 78% for the monoiodinated peptide.

Integrin Binding Assays. The ability of cyclopentapeptide **3** to compete with [^{125}I]echistatin for binding to pure $\alpha_v\beta_3$ integrin isolated from human placenta was evaluated in solid phase assays.[15] IC_{50} values showed a binding affinity of compound **3** toward $\alpha_v\beta_3$ integrin of 48.0 ± 1.2 nM, slightly lower than that of peptide **1** (IC_{50} 6.5 ± 2.0 nM) (Figure 2).[15]

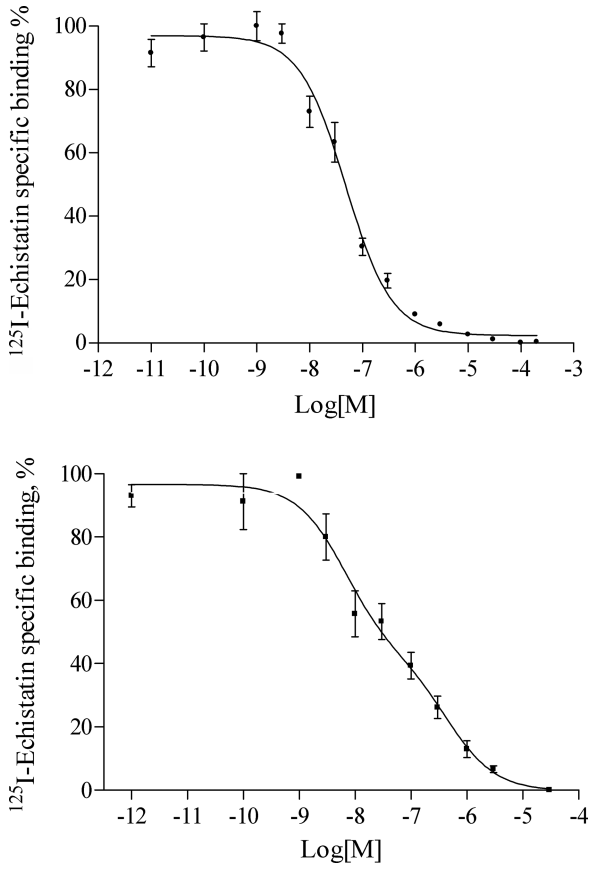

Figure 2. Morpholine-based RGD-cyclopeptides: D-Mor-containing compound **1**, ^{127}I-D-Mor-D-Tyr-containing compound **3**. Data are presented as means ± SD from three independent experiments, and error bars represent 95% confidence interval.

Data analyses indicates that compound **3** binds to $\alpha_v\beta_3$ integrin according to a one-site binding model (Hill slope −0.92 for one-site model), whereas cyclopeptide **1** showed binding to $\alpha_v\beta_3$ integrin according to a two-site binding model (Hill slope −0.56 for one-site model), thus suggesting that the iodotyrosine-derived ligand **3** displays a different affinity profile toward $\alpha_v\beta_3$ integrin.[15]

Molecular Modeling. To understand the potential differences in binding mode of cyclopeptide **3** to $\alpha_v\beta_3$ integrin, as compared to ligand **1**, a docking simulation was carried out.[15] The crystal structure of the complex formed by *c*[RGDf(Me)V] and the extracellular fragment of $\alpha_v\beta_3$ integrin (PDB code: 1L5G) provides a general mode of interaction between the integrin and its ligands.[16] Asp carboxylate and Arg guanidinium moieties of RGD-based ligands are key structural elements for receptor recognition. The carboxylate group interacts with the metal ion-dependent adhesion site (MIDAS) of the Mn^{2+} ion and Ser121/Ser123, whereas the Arg guanidinium group is responsible for salt bridge interactions with Asp218 and Asp150 side chains. Additional ligand−receptor contacts occur between Tyr122 in hydrophobic π-stacking and Asn215. The docking program Autodock 4.0.1[17] was used to evaluate the binding energies of selected conformations of ligand **3**.[18] Docked conformations were analyzed by taking into account the binding interactions as observed in the crystal structure of the bound ligand−protein complex. Docking calculations resulted in a cluster of conformations characterized by key interactions with Asp218 and the MIDAS site of the integrin, thus confirming these interactions as necessary for the molecular recognition of Arg−Gly−Asp-containing ligands (Figure 3).

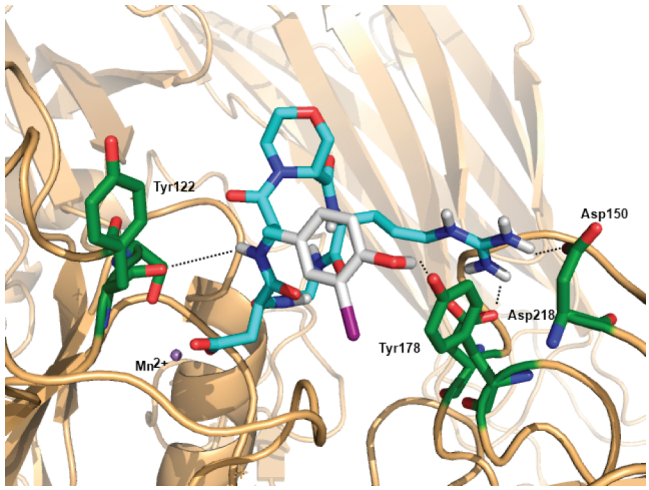

Figure 3. RGD ligand **3** (cyan) docked into the binding region of $\alpha_v\beta_3$ integrin, highlighting protein residues (green) that form key interactions (dotted lines): Asp218 vs Arg, Ser121 and Mn^{2+} vs Asp, Tyr122 and Tyr178 vs D-I-Tyr. Nonpolar hydrogen atoms are omitted for clarity.

Ligand **3** showed that the Asp side chain is located in the MIDAS site and interacts with Ser121 and guanidinium group of Arg, undergoes a salt-bridge interaction with Asp218, and a monodentate interaction with Asp150. The main conformation of the cluster showed a different orientation of the D-Tyr aromatic ring, not facing Tyr-122 in a π-stacking interaction, as observed for compound **1**, but displaying a hydrogen-bond between the Tyr OH group of the aromatic side chain and the OH group of Tyr-178 as hydrogen-bond acceptor. The NH group of D-Tyr showed a hydrogen bond with the Tyr-122 CO group. Thus, a different binding mode geometry was assessed for compound **3** as a result of D-Tyr side chain, possibly relating to a different binding profile with respect to compound **1** (Figure 2).

Cell Biology Assays. *Adhesion and Migration of A375 M Melanoma Cells in the Presence of Morpholine-Based RGD-Cyclopeptides 1−3.* A375 M human melanoma cells express a wide variety of integrin subunits (α_V, β_3, β_5, α_5, β_1) and a high level of $\alpha_v\beta_3$ heterodimer.[12g] Figure 4 shows the ability of ligands **1**, **2**, and **3**, used at final concentrations of 10, 1.0, or 0.1 μM, to inhibit the binding of A375 M melanoma cells to various RGD-containing substrates, such as vitronectin and fibronectin. Tests were performed in the presence of 2 mmol/L $MnCl_2$, in order to switch integrins of tumor cells into the activated form.[6c] Figure 4 also shows that ligand **1** inhibits the binding of melanoma cells to vitronectin to a great extent,

dx.doi.org/10.1021/jm2016232 | J. Med. Chem. 2012, 55, 5024−5033

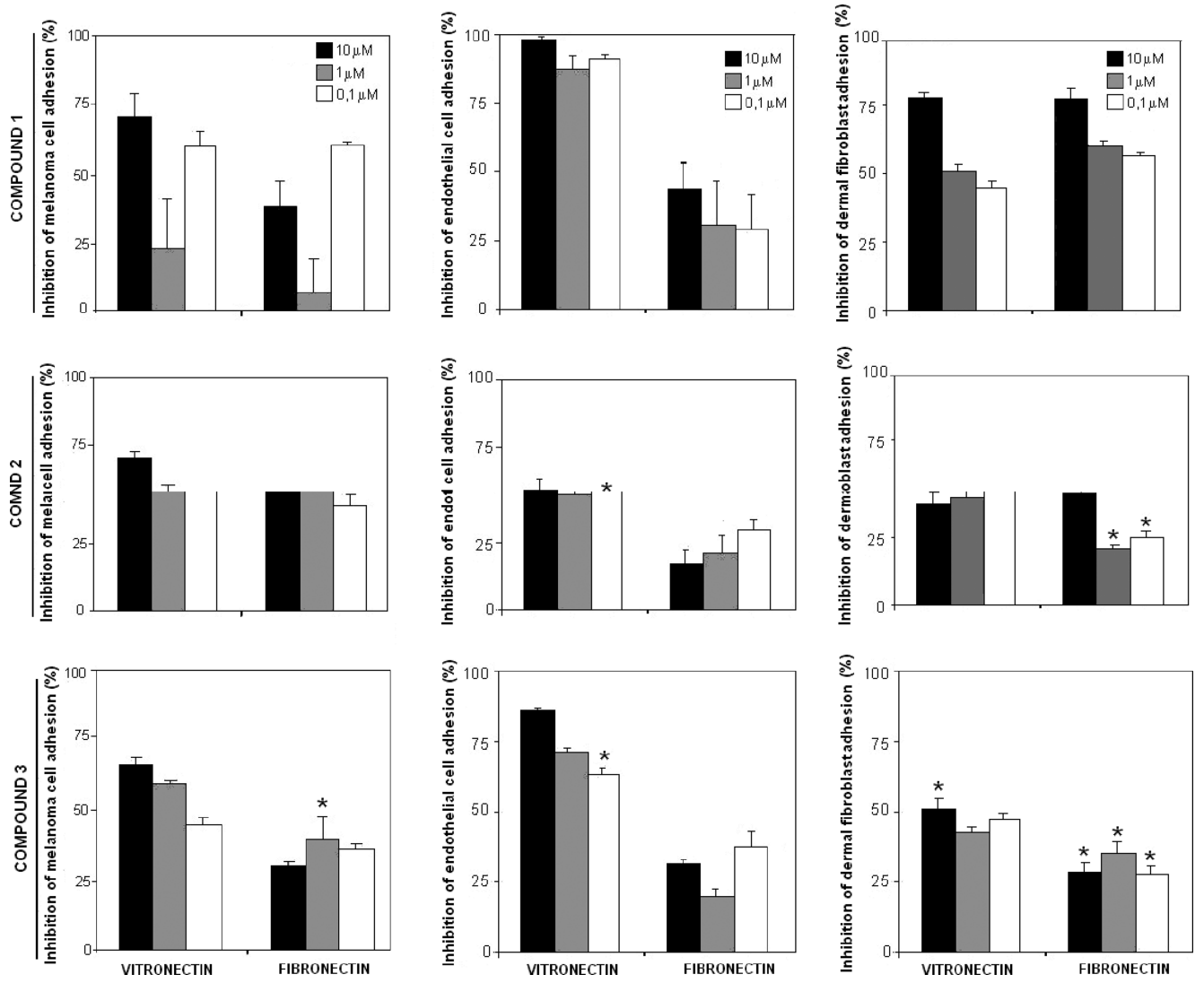

Figure 4. Adhesion of A375 M melanoma cells, HUVECs and dermal fibroblasts to vitronectin, and fibronectin in the presence of compounds **1**, **2**, or **3**. The values are expressed as % inhibition ± SEM of cell adhesion relative to control (untreated cells). Significantly different at $p < 0.05$ as compared to compound **1**.

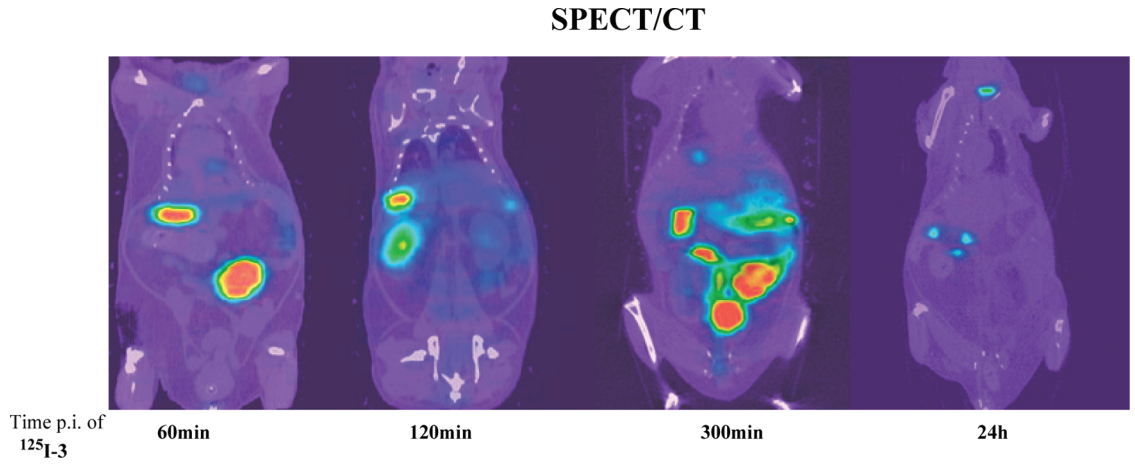

Figure 5. Radioactivity biodistribution evaluated in a healthy mouse at 60, 120, and 300 min and 24 h after ^{125}I-**3** injection.

whereas the inhibition of cell adhesion to fibronectin is less effective. Ligands **2** and **3** expressed an inhibitory ability on tumor cell adhesion comparable to that of ligand **1**. These results suggest that ligands **1**, **2**, and **3** display a quite comparable affinity for $\alpha_v\beta_3$ integrin, and the addition of iodine does not modify the affinity in living cells. A "scratch wound"

dx.doi.org/10.1021/jm2016232 | J. Med. Chem. 2012, 55, 5024–5033

model was used to examine the effect of D-morpholine-containing RGD-ligands on in vitro migration of melanoma cells. Tumor cells exposed to ligands **1**, **2**, and **3** did not modify their migration rate with respect to nonexposed tumor cells (control tumor cells). The migration rate (as represented by the reduction of scratch width) and the morphology of tumor cells exposed to D-morpholine-containing RGD-ligands were found comparable at 10 μM, 1 μM, and 10 nM concentration of the ligand, with respect to control tumor cells (Figure S2, Supporting Information).

*Adhesion and in Vitro Tubulogenesis of HUVEC in the Presence of Morpholine-Based RGD-Cyclopeptides **1**–**3**.* IL-1β-stimulated HUVECs express integrin subunits (α_v, β_3, β_5, α_5, β_1) and $\alpha_v\beta_3$ heterodimer. Ligands **1**, **2**, and **3** suppressed the adhesion of IL-1β-stimulated HUVECs to vitronectin, whereas they did not completely suppress the adhesion of activated endothelial cells to fibronectin (Figure 4). We can speculate that D-morpholine-based RGD-cyclopeptides act preferentially on the endothelial $\alpha_v\beta_3$ integrin instead of the $\alpha_5\beta_1$ integrin. To assess whether ligands **1**, **2**, and **3** were able to exert an antiangiogenic activity, we examined the ability of these peptides to repress in vitro tube formation by HUVEC, seeded on a Matrigel layer. Figure S3 of Supporting Information shows that tube formation by HUVEC was not inhibited by D-morpholine-containing RGD-ligands.

Adhesion of HDFs in the Presence of Morpholine-Based RGD-Cyclopeptides. As shown in Figure 4, ligand **1** suppressed the adhesion of HDFs to vitronectin and fibronectin with a high efficiency, whereas ligand **2** and **3** expressed a significantly reduced efficiency.

Biodistribution and Melanoma Imaging. The radioactivity distribution was evaluated in a nontumor-bearing mouse at 60, 120, and 300 min and 24 h post injection (pi) (Figure 5). The accumulation in gallbladder and kidneys remained consistent for at least two hours pi, and the tracer was excreted via renal and hepatobiliary routes, allowing for a fast clearance of nonspecific bound tracer. Accumulation in the spleen might be due to the structural similarity of integrin $\alpha_v\beta_3$ to $\alpha_{IIb}\beta_3$ integrin expressed on spleen-enriched platelets. The release of the ^{125}I atom from the molecule and its accumulation in the thyroid gland increased with time, a phenomenon that can be avoided by the preadministration of a solution of KI (4 mg/L). At 24 h pi, little radioactivity remained in the organism, mainly in the thyroid and bowel.

Figure 6 shows the localization of the ^{125}I-**3** compound in the site of the implanted tumor as determined by micro SPECT-CT imaging. The images clearly show that the ^{125}I-**3** ligand has the capacity to monitor in vivo the growth of $\alpha_v\beta_3$ integrin-positive melanoma cells. Binding studies showed a good displacement of the radiotracer by the parent nonradioactive compound, with a mean ratio of saturated to displaced receptors in tumor tissue of 5.753 ± 0.6 and having the controlateral muscle as the reference tissue.

DISCUSSION AND CONCLUSIONS

As reported, $\alpha_v\beta_3$ integrin-targeted radiotracers are able to reveal a tumor mass and to monitor growth and diffusion of tumor cells.[19] We tested D-morpholine-based RGD-cyclopentapeptides **1**, **2**, and **3** in in vitro and in vivo assays, and they were found to inhibit the adhesion of human melanoma cells to RGD substrates, such as vitronectin and fibronection. These ligands proved to be more specific for $\alpha_v\beta_3$ than $\alpha_5\beta_1$ integrin. "Scratch wound" experiments revealed that melanoma cells exposed to ligands **1**, **2**, and **3** did not modify their migration rate as compared to nonexposed tumor cells. Several interactions operate between tumor cells and the extracellular matrix, thus the inhibition of $\alpha_v\beta_3$ integrin-mediated cell adhesion per se might not be sufficient to influence tumor cell migration.[6c,20] Ligands **1**, **2**, and **3** also repressed the adhesion of IL-1β-stimulated HUVEC to vitronectin, whereas inhibition of endothelial cell adhesion on fibronectin was not significant. At the same time, ligands **1**, **2**, and **3** did not block in vitro capillary-like tube formation by HUVEC. We assume that the reduced affinity of D-morpholine-based RGD-cyclopentapeptides for $\alpha_5\beta_1$ integrin fails to influence in vitro angiogenesis. Indeed, it has been found that only simultaneous inhibition of both integrins reduces capillary tube formation.[11,12h,21]

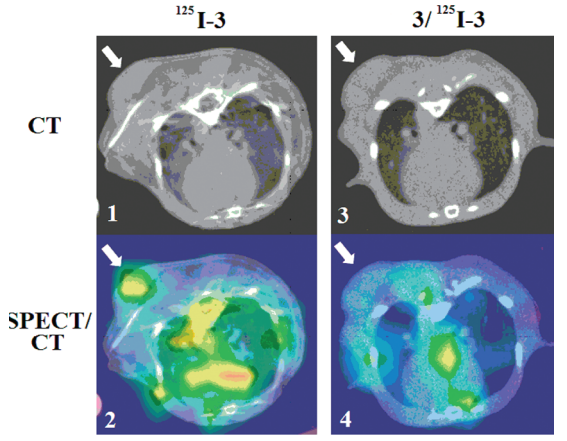

Figure 6. Transaxial slices through mouse chest at implanted melanoma tumor level (arrows). In upper panels CT images, in lower panels fused CT and SPECT images. Images were acquired at 40 min after tail vein injection of ^{125}I-**3** (250 μCi in 0.2 mL of saline). The displacement study was achieved with an excess of cold ligand (18 mg/kg) injected 10 min before the tracer.

Tumor cells recruit host inflammatory and stromal cells, which generate a microenvironment able to promote growth and dissemination of cancer cells.[22] Because fibroblasts represent the most abundant host cells within a tumor microenvironment,[23] we injected a suspension of tumor cells and $\alpha_v\beta_3$ integrin expressing HDF into immunodeficient mice to test in vivo behavior of ^{125}I-**3** ligand by micro-SPECT/CT analysis. We found a high tracer retention within the tumor mass with a satisfying tumor to background ratio. Co-injection of ^{125}I-**3** and the corresponding unlabeled ligand **3** showed high selectivity of this ligand for $\alpha_v\beta_3$ expressing tumor cells.

Thus, the ^{125}I-**3** ligand may represent a new radiopharmaceutical with the potential of early detection of a tumor mass and of monitoring the therapeutic response. Moreover, high affinity of this radiotracer for $\alpha_v\beta_3$ integrin, which is characteristic of tumor endothelial cells, can be a valuable diagnostic tool in a large population of cancers, including tumors with low level of $\alpha_v\beta_3$-expressing cells. These considerations extend the applications of ^{125}I-**3** from melanoma to several tumor histotypes.

Finally, the D-Mor-containing cyclopentapeptide ligand **3** might be used in novel therapeutic strategies upon labeling with ^{131}I radioisotope.

EXPERIMENTAL SECTION

General. H-Gly-2-Cl-Trt resin (1.1 mmol/g) was purchased from Fluka. Chromatographic separations were performed on silica gel

dx.doi.org/10.1021/jm2016232 | J. Med. Chem. 2012, 55, 5024–5033

Table 1. ^{1}H and ^{13}C Chemical Shifts of 2 and 3 in DMSO-d_6 Solutions at 298 K

	^{1}H, 2	^{1}H, 3		^{13}C, 2	^{13}C, 3
H-2	4.28; 3.37	4.28; 3.34	C-2	68.8	69.0
H-3	4.59	4.66	C-3	53.5	53.7
H-5	3.08	3.16; 3.08	C-5	66.8	66.4
H-6	3.93; 3.70	3.90; 3.72	C-6	68.2	68.4
Gly NH	8.73	8.61			
Arg NH	7.40	8.56			
Asp NH	8.65	8.66			
D-Tyr NH	7.19	7.35			
Gly H-α	4.07	3.99; 3.10	Gly C-α	44.5	44.1
Arg H-α	3.99	4.01	Arg C-α	53.3	53.7
Arg H-β,γ	1.65; 1.50	1.63; 1.43	Arg C-β,γ	24.9; 22.0	24.8; 21.2
Arg H-δ	3.04	3.06	Arg C-δ	40.5	40.1
Asp H-α	4.78	4.71	Asp C-α	57.0	56.7
Asp H-β	2.82; 2.70	2.88; 2.56	Asp C-β	39.6	39.8
D-Tyr H-α	4.47	4.51	D-Tyr C-α	49.4	50.4
D-Tyr H-β	2.14	2.32	D-Tyr C-β	28.7	35.8
D-Tyr H-Ar	6.95; 6.60	7.66; 7.34; 7.24	D-Tyr C-Ar	115.3; 130.1	115.8; 129.8; 139.1

(Kieselgel 60, Merck) using flash-column techniques. R_f values refer to TLC carried out on 25 mm silica gel plates (Merck F254) with same eluant as for column chromatography. Solid-phase reactions were carried out on a shaker using solvents of HPLC quality. Bromophenol Blue (BB) test was performed as follows: a small amount of resin beads were suspended in a vial with 0.5 mL of DMF, two drops of a 1% solution of bromophenol blue in dimethylacetamide were added, and the sample was observed. The BB test was considered positive (presence of free amino groups) when the resin beads turned blue and negative (absence of free amino groups) when the beads remained colorless. ESI mass spectra were carried out on a ion-trap double quadrupole mass spectrometer using electrospray (ES^+) ionization techniques, and a normalized collision energy within the range of 25–32 eV for MSMS experiments. Ligands **2** and **3** were purified by Beckman-Gold HPLC system equipped with a reverse-phase column (Alltima C18 10 μm, 250 mm × 10 mm, Alltech) using H_2O/CH_3CN gradient eluant buffered with 0.1% TFA (flow rate 2.5 mL/min, λ 254 nm, gradient eluant: CH_3CN 10%/5 min, CH_3CN 10–90%/25 min). Analytical HPLC analyses were performed on Dionex Ulltimate 3000 system equipped with a reverse-phase column (Alltima C18 5 μm, 250 mm × 4.6 mm, Alltech) and the same gradient eluant. Ligand ^{125}I-**3** was purified by Beckman-Gold HPLC system equipped with a reverse-phase column (C-8 Waters Spherisorb S5 250 mm × 4.6 mm) and the same gradient eluant. $Na^{125}I$ in 0.2N NaOH solution was purchased from PerkinElmer (10 μL, 100 mCi/mL, 17 Ci (629GBq)/mg, ^{125}I 97%, ^{126}I < 3%, radiochemical purity >99%, carrier free). HPLC analysis was used to determine purity and all tested compounds possessed >95% purity.

***c*[RGDy-(3*R*)-carboxymorpholine] (2).** H-Gly-2-Cl-Trt resin (466 mg, 0.5 mmol) was used as starting material. Fmoc-deprotections and completion of each coupling reaction were assessed by performing a BB test. Coupling was performed with a solution consisting of *N*-Fmoc-Arg(Pbf)-OH (973 mg, 1.5 mmol, 3 equiv), HOBt (203 mg, 1.5 mmol, 3 equiv) in DMF (3 mL), and DIC (203 μL, 1.5 mmol, 3 equiv) was added dropwise, at 0 °C. The resulting mixture was stirred for 10 min at 0 °C and for a further 10 min at room temperature and then was added to the resin. This mixture was shaken at room temperature for 24 h. The solution was drained, and the resin was sequentially washed with 5% DIPEA in DMF (3 × 5 mL) and DMF (5 × 5 mL). Fmoc deprotection was performed with 30% piperidine in DMF (10 mL) for 30 min, followed by resin washings with DMF (3 × 10 mL). After deprotection, H-Arg(Pbf)-Gly-2-Cl-Trt resin was suspended in a solution of HOBt (356.8 mg, 2.64 mmol, 6 equiv), DIC (415.6 μL, 2.64 mmol, 6 equiv), and *N*-Fmoc-(*R*)-morpholine-3-carboxylic acid (465 mg, 1.32 mmol, 2.64 equiv) in DMF (3 mL) and shaken for two days. The solution was drained, and resin was washed with 5% DIPEA in DMF (3 × 5 mL) and DMF (5 × 5 mL). After deprotection, H-(3*R*)-carboxymorpholine-Arg(Pbf)-Gly-2-Cl-Trt resin was suspended in a solution of HOBt (405 mg, 3 mmol, 6 equiv), DIC (472 μL, 3 mmol, 6 equiv), and *N*-Fmoc-D-Tyr(*t*-Bu)-OH (689 mg, 1.5 mmol, 3 equiv) in DMF (3 mL) and shaken for three days. The solution was drained and the resin washed with 5% DIPEA in DMF (3 × 5 mL) and DMF (5 × 5 mL). After deprotection, H-D-Tyr(*t*-Bu)-(3*R*)-carboxymorpholine-Arg(Pbf)-Gly-2-Cl-Trt resin was suspended in a solution of TBTU (802.7 mg, 2.5 mmol, 5 equiv), *N*-Fmoc-Asp(*t*-Bu)-OH (1.028 g, 2.5 mmol, 5 equiv), and DIPEA (428 μL, 2.5 mmol, 5 equiv) in DMF (3 mL) and shaken for three days. The solution was drained and resin washed with 5% DIPEA in DMF (3 × 5 mL) and DMF (5 × 5 mL). *N*-Fmoc-Asp(*t*-Bu)-D-Tyr(*t*-Bu)-(3*R*)-carboxymorpholine-Arg(Pbf)-Gly-2-Cl-Trt resin was deprotected and washed with DMF (5 × 5 mL) and DCM (5 × 5 mL). In a solid-phase reaction vessel H-Asp(*t*-Bu)-D-Phe-(3*R*)-carboxymorpholine-Arg(Pbf)-Gly-2-Cl-Trt resin was treated with 5 mL of 1% TFA/DCM solution (10 × 2 min). The filtrates were immediately neutralized with a 10% pyridine/MeOH solution (1 mL), and then the resin was washed with DCM (3 × 5 mL). Fractions (TLC eluant 4:1 DCM/MeOH) were combined and concentrated under reduced pressure to yield a residue, which was suspended in H_2O and purified from the pyridinium salts by size-exclusion chromatography (AMBERLITE XAD2 resin, H_2O then MeOH). Evaporation of combined MeOH fractions containing the product afforded the side-chain protected compound (493 mg, 33%) as a white solid material. The linear peptide (493 mg, 0.5 mmol) was dissolved under a nitrogen atmosphere in DMF (120 mL), HATU (152.1 mg, 0.4 mmol, 0.8 equiv), and TBTU (354 mg, 1.1 mmol, 2.2 equiv) and DIPEA (257 μL, 1.5 mmol, 3 equiv) were added. The resulting mixture was stirred for two days at room temperature. The solvent was distilled off under reduced pressure, and the residue was dissolved in H_2O (60 mL) and extracted with EtOAc (3 × 80 mL). The organic phase was washed twice with 5% $NaHCO_3$, dried with Na_2SO_4, and evaporated under reduced pressure. The crude residue was purified by flash column chromatography (9:1 DCM–MeOH, R_f 0.37) to give the protected cyclic peptide (140 mg, 30%) as a yellow solid material. HPLC: t_R = 24.30, purity 97%. Side chain protected cyclic peptide (140 mg, 0.15 mmol), was treated with 95:2.5:2.5 TFA/H_2O/TIS mixture (20 mL) for 2 h. The reaction mixture was evaporated under reduced pressure, and the residue was dissolved in H_2O (60 mL). The aqueous phase was washed with $^{i}Pr_2O$ (3 × 60 mL) and freeze-dried. The crude residue was purified by semi-preparative HPLC to give the side-chain deprotected **2** (30 mg, 34%), as a white solid. Trifluoroacetate ion was replaced with chloride ion by ion-exchange chromatography (AMBERLITE IRA-96 resin, chloride form). See Table 1 for ^{1}H and ^{13}C NMR data. ESI-MS *m*/*z* 605.14 (M + H^+, 100). ESI-MSMS *m*/*z* 605.5 (M + H^+, 1), 588.0 (100), 577.0 (30), 570.0 (17), 559.9 (42), 546.0 (11), 533 (12), 520.0 (72). Anal.

dx.doi.org/10.1021/jm2016232 | J. Med. Chem. 2012, 55, 5024–5033

Calcd for $C_{26}H_{37}ClN_8O_9$: C, 48.71; H, 5.82; N, 17.48. Found: C, 48.88; H, 5.91; N, 17.32. HPLC: t_R = 12.1, 95% purity.

***c*[RGD-(3′I-y)-(3*R*)-carboxymorpholine] (3).** A solution of ligand **2** (12.0 mg, 0.020 mmol) in PBS (2 mL) was added to sodium iodide (3.07 mg, 0.020 mmol), followed by chloramine-T hydrate (4.66 mg, 0.020 mmol). The reaction mixture was stirred at room temperature for 20 min and then quenched with a solution of 5% sodium metabisulphite (0.8 mL). The mixture was extracted with DCM (3 × 5 mL) and loaded on a preconditioned C18 Sep-pak column. The C18 column was washed with water (6 mL) and subsequently eluted with MeOH. The crude product was purified by semipreparative HPLC to obtain ligand **3** (4.67 mg, 32%). See Table 1 for ^{1}H and ^{13}C NMR data. ESI-MS m/z 731.25 (M + H$^+$, 100). ESI-MSMS m/z 731.2 (M + H$^+$, 15), 714.1 (100), 685.9 (39), 672.1 (22), 646.1 (76). Anal. Calcd for $C_{26}H_{36}ClIN_8O_9$: C, 40.72; H, 4.73; N, 14.61. Found: C, 40.81; H, 4.83; N, 14.12. HPLC: t_R = 15.2, 96% purity.

***c*[RGD-(3′^{125}I-y)-(3*R*)-carboxymorpholine] (^{125}I-3).** A solution of PBS (100 μL, 0.05 M) containing Na^{125}I (20 μL, 2 mCi, 0.918 nM), peptide **2** (10 μL of a 0.05 M PBS solution, 16.5 nmol), and chloramine-T (1.88 μL of a freshly prepared 0.05 M PBS solution, 8.24 nmol, 9 equiv) was prepared. The reaction mixture was stirred at room temperature for 20 min and then quenched by adding a solution of sodium metabisulphite (2.18 μL of a freshly prepared 0.05 M PBS solution, 8.24 nmol, 9 equiv). The mixture was extracted with DCM (3 × 0.5 mL) and purified by HPLC, and the radioactivity of fractions collected every 30 s was determined with a γ-counter (Supporting Information Figure S1). Fractions containing the chemically pure ^{125}I-**3** were pooled together (1.55 mCi, 78% radiochemical yield) and used for in vivo experiments after solvent removal. HPLC: t_R = 15.2, 98% radiochemical purity, >99% chemical purity.

Solid-Phase Integrin Binding Assay. [^{125}I]-Echistatin, labeled by the lactoperoxidase method[24] to a specific activity of 2000 Ci/mmol, was purchased from GE Healthcare, and integrin $\alpha_v\beta_3$ from human placenta was purchased from Chemicon International Inc., Temecula, CA.

Purified $\alpha_v\beta_3$ integrin was diluted in coating buffer (20 mM Tris (pH 7.4), 150 mM NaCl, 2 mM $CaCl_2$, 1 mM $MgCl_2$, 1 mM $MnCl_2$) at concentrations of 500 or 1000 ng/mL. An aliquot of diluted integrin (100 μL/well) was added to a 96-well microtiter plate (Optiplate-96 HB, PerkinElmer Life Sciences, Boston, MA), and plates were incubated overnight at 4 °C. Plates were washed once with blocking/binding buffer (20 mM Tris (pH 7.4), 150 mM NaCl, 2 mM $CaCl_2$, 1 mM $MgCl_2$, 1 mM $MnCl_2$, 1% BSA) and incubated at room temperature for additional 2 h. Plates were rinsed twice with same buffer, and then competition binding assays were performed with a constant concentration of [^{125}I]-Echistatin (0.05 nM). Concentrations of tested compound ranged from 0.01 to 100 nM. All assays were performed in triplicate in a final volume of 0.2 mL, each containing the following species: 0.05 mL of [^{125}I]-Echistatin, 0.04 mL of tested compound, and 0.11 mL of blocking/binding buffer. Nonspecific binding was defined as [^{125}I]-Echistatin bound in presence of an excess (1 μM) of unlabeled echistatin. After incubation at room temperature for 3 h, plates were washed three times with blocking/binding buffer and counted in a Top-Count NXT microplate scintillation counter (PerkinElmer Life Sciences, Boston, MA) using 200 μL/well of MicroScint-40 liquid scintillation (PerkinElmer Life Sciences, Boston, MA).

Data are shown as means ± SD from three independent experiments. IC_{50} values were determined by fitting binding inhibition data by nonlinear regression using GraphPad Prism 4.0 Software Package (GraphPad Prism, San Diego, CA).

Cell Lines and Culture Conditions. The A375 M human melanoma cell line was obtained from the American Type Culture Collection (ATCC, Rockville, MD).[12g] Human dermal skin fibroblasts (HDF) were kindly donated by Dr. Daniela Monti, Department of Experimental Pathology and Oncology, University of Florence. Melanoma cells and HDF were grown in Dulbecco's Modified Eagle Medium, containing 4500 mg/L glucose (DMEM 4500, GIBCO) supplemented with 10% fetal calf serum (FCS) at 37 °C in a humidified incubator containing 10% CO_2. Then 5.0 × 10^5 melanoma cells or 1 × 10^6 HDF were seeded in 100 mm dishes and propagated every 3 days by incubation with a trypsin−EDTA solution. Cultures were periodically monitored for mycoplasma contamination. Primary cultures of human umbilical vein endothelial cells (HUVEC) were obtained from Lonza (USA). HUVEC grown in endothelial cell growth medium-2 (EGM-2) containing endothelial cell growth supplements were subcultivated using a trypsin-EDTA solution, 1:3 split ratio. Cells between passages 2 and 4 grown to confluence in plates coated with 1% bovine gelatin (Sigma, St. Louis) were used in the experiments.

RNA Isolation and Polymerase Chain Reaction (PCR). Total RNA extracted using RNAgents (Total RNA Isolation System, Promega, Madison, WI) was determined spectrophotometrically. Complementary DNA (cDNA) was synthesized from 2 μg of total RNA using 1 μL of ImProm-II reverse transcriptase (Promega). Aliquots of 2 μL of the cDNA were used for PCR amplification. The specific primers used for the identification of human α_v, α_5, β_1, β_3, β_5, and GAPDH are reported in Table S1 of Supporting Informations. All PCR experiments were conducted using 0.05 U/μL of Go-Taq Polymerase (Promega). Amplification was carried out on a Perkin-Elmer Thermal cycler. Then 8 μL of each PCR products were visualized after electrophoresis in a 2% agarose gel containing 0.5 μg/mL of ethidium bromide. cDNA products were evaluated on the basis of a standard PCR marker.

Flow Cytometry Assay. Tumor cells were detached by gentle treatment with Accutase, a 0.5 mM EDTA solution, washed, and incubated for 1 h at 4 °C in the presence of anti $\alpha_v\beta_3$ monoclonal antibody (1 μg/50 μL, Anti-Integrin $\alpha_v\beta_3$, clone LM609, Millipore). Cells were then washed and incubated for 1 h at 4 °C with a secondary antibody, 5 μg/mL goat antimouse IgG conjugated with FITC (Santa Cruz Biotechnology, Inc., Santa Cruz, CA). $\alpha_v\beta_3$ -positive cells were analyzed at 488 nm on the flow cytometer FACScan system (BD-FACS Canto).

Cell Adhesion Assay. Plates (96 wells) were coated with fibronectin (1 μg/mL) or vitronectin (10 μg/mL) by overnight incubation at 4 °C and then incubated at 37 °C for 1 h with 1% BSA in PBS. Melanoma cells, IL-1β (400 U/mL)-stimulated HUVECs, or human dermal fibroblasts (HDF) were resuspended in serum-free medium and exposed to ligands **1**, **2**, or **3** (final concentration was 0.1, 1, or 10 μM) at 37 °C for 30 min to allow for ligand−integrin equilibrium to be reached. Melanoma cell adhesion assays were performed in the presence or in the absence of 2 mmol/L $MnCl_2$. Cells were plated (4−5 × 10^4 cells/well) and incubated at 37 °C for 2 h. Nonadherent cells were removed with PBS, and adherent cells were stained with 0.5% crystal violet solution in 20% methanol. After 2 h of incubation at 4 °C, plates were examined at 540 nm in a counter ELX800 (Biotek Instruments). Experiments were conducted in triplicate and repeated at least three times. Data are presented as means ± SD from three independent experiments.

Animal Model and Study Design. In vivo experiments were conducted in accordance with national guidelines and approved by the Ethical Committee of the Animal Welfare Office of the Italian Work Ministry and conforming to legal mandates and Italian guidelines for care and maintenance of laboratory animals. Eighteen-week-old SCID bg/bg mice (Charles River Laboratories International) were injected subcutaneously in the shoulder area with a suspension of melanoma cells and 20 ng/mL TGFβ-activated fibroblasts. Then 1 ×10^6 A375 M melanoma cells and 0.5 × 10^6 HDF were previously resuspended in 100 μL of PBS diluted 1:1 with a Matrigel solution (BD Biosciences). Animals were kept under pathogen-free conditions and allowed to feed freely. Tumor growth was monitored daily.

Small-Animal SPECT and CT Studies. In vivo studies were conducted using a "hybrid" imaging system for small laboratory animals allowing for the study of biological processes using minimally invasive procedures. Engrafted tumor tracer uptake was studied at different time-points after tail vein injection. Binding specificity to integrin receptors was evaluated by in vivo displacement studies, in which a high dose of cold tracer was injected 10 min before radiolabeled one. Imaging studies were performed using the Flex

Triumph preclinical imaging system, which combines positron (PET) and single-photon emission (SPECT) tomography with the emission tomography (CT) for anatomic coregistration (GE Healthcare/Gamma Medica-Ideas, Waukesha, WI). ^{125}I-iodinated tracers ^{125}I-**3** was studied in vivo by SPECT, allowing for use directly the in vitro tracer data to the in vivo experimentation. Imaging studies required monitoring of anesthetized animals throughout the imaging procedure, and anesthesia was conducted in accordance with National Guidelines and approved by the Ethical Committee. Given that anesthesia in general causes hypothermia in small animals, appropriate warming was provided during imaging procedure by using a heating bed set at 37 °C. Physiological monitoring was achieved by measuring respiration rate with a pressure pad placed under the mouse abdomen. Saturation experiments (SE) to visualize tumors and displacement experiments (DE) were performed. In SE, ^{125}I-**3** (7−10 MBq in 200 μL of physiological saline) was injected via tail vein into tumor bearing animals kept under anesthesia. After 30 min, a CT aquisition was performed, followed by SPECT scan, starting at 40 min pi. CT scan was acquired with 50 kV and 320 μA tube settings. The magnification factor was set to 2, resulting in an axial field of view of 59.2 mm. 512 projections, 500 μs each, were acquired on a circular orbit in 256 s with an acquisition matrix of 1184 × 1120, 100 μm, pixel. SPECT projections were acquired with a 5-pinhole high-resolution collimator (1 mm hole diameter, 75 mm focal distance) with radius of rotation of 40 mm resulting in an axial field of view of 52.9 mm. then 64 projections, 20 s each, were acquired on a circular orbit for a total acquisition time of about 22 min. Acquisition matrix was 80 × 80, 1.5 mm pixel size. Energy window was set on the ^{125}I photopeak ranging from 20 to 36 KeV. The DE were performed by injecting 18 mg/kg of compound **3** 10 min before injection of tracer. Once scanning was complete, the animals were recovered in a housing unit and monitored until awake.

Data Analysis of Small-Animal SPECT and CT Studies. CT image data set was reconstructed using a cone-beam FBP algorithm (FDK) and an optimum noise filter. Reconstruction matrix was 512 × 512 × 512, 180 μm pixel size. SPECT images were reconstructed with ordered subset expectation maximization algorithm (8 subsets and 5 iterations) and a reconstruction matrix of 60 × 60 × 60, 1.5 mm pixel size. No correction for radiation attenuation and scatter was applied. Fused images were visually analyzed to detect the engrafted tumor mass, and regional SPECT activities were measured using the analysis software Vivid (Gamma Medica-Ideas, Northridge, CA) by delineating the region of interest (ROI) of tumor in fused CT images. A similar ROI was generated for muscle tissue on contralateral side of tumor. Tumor ROI activity was normalized (nTA) with the following formula:

$$n\mathrm{TA} = \frac{\mathrm{TA} - \mathrm{BA}}{\mathrm{BA}}$$

where TA is tumor activity and BA is background activity measured in muscle tissue contralateral to tumor.

Docking Calculations. Automated docking studies were carried out by Autodock 4.0.1 program,[17] using the Lamarckian Genetic Algorithm (LGA) as a search engine. The AutoDockTools 1.4.5 (ADT) graphical interface[25] was used to prepare integrin and ligands PDBQT files. Coordinates of ligand **3** were retrieved from lowest energy conformers resulting from molecular mechanics calculations starting from geometry of ligand **1**, whereas coordinates of $\alpha_v\beta3$ receptor were retrieved from the Protein Data Bank (PDB code: 1L5G), and ligand−protein complex was unmerged for achieving free receptor structure. Water molecules were removed. For protein receptor and ligand **3**, all hydrogens were added, Gasteiger charges were computed, and nonpolar hydrogens were merged. A charge value of +2.0 to each Mn atom of protein receptor was successively added. Three-dimensional energy scoring grids of 0.375 Å resolution and 40 Å × 40 Å × 40 Å dimensions were computed. Center of grid was set to be coincident with mass center of ligands preliminary fitted on the X-ray structure of *c*[RGDf(Me)V] in the $\alpha v\beta3$ complex (1L5G). A total of 50 runs with a maximum of 2500000 energy evaluations were carried out for each ligand, using the default parameters for LGA. Cluster analysis was performed on docked results using a root-mean-square (rms) tolerance of 1.5 Å. Analysis of binding mode, calculation of binding energy, and prediction of binding activity of docked conformations were carried out using PyMol Autodock Tools plugin within PyMol software.[26]

■ ASSOCIATED CONTENT

Ⓢ Supporting Information

Additional experimental methods, radiochromatogram of ^{125}I-**3**, and additional cell biology assays data. This material is available free of charge via the Internet at http://pubs.acs.org.

■ AUTHOR INFORMATION

Corresponding Author

*For A.G.: phone, +39 055 4573481; fax, +39 055 4573569; E-mail, antonio.guarna@unifi.it. For A.P.: phone, +39 055 7947527; fax, +39 055 4224392; E-mail, a.pupi@dfc.unifi.it. For L.C.: phone, +39 055 4598207; fax, +39 055 4598900; E-mail, lido.calorini@unifi.it.

Notes

The authors declare no competing financial interest.

■ ACKNOWLEDGMENTS

This work has received financial support from the Istituto Toscano Tumori and MIUR (PRIN08, Grant 2008J4YNJY_003). Also, financial contributions from CINM-PIS, University of Florence, and Fondazione Roma are acknowledged. Dr. Alessandro Sisti is acknowledged for carrying out preliminary labeling experiments. Ente Cassa di Risparmio is acknowledged for the granting the MicroPET/SPECT/CT instrument.

■ ABBREVIATIONS USED

SPECT, single positron emission computed tomography; PET, positon emission tomography; RGD, Arg-Gly-Asp; VGP, vertical growth phase; CT, computed tomography; VN, vitronectin; FN, fibronectin; HUVEC, human umbilical vein endothelial cells; IL-1*β*, interleukin-1*β*; ESI-MSMS, electropray ionization tandem mass spectrometry; EGM-2, endothelial cell growth medium-2; EDTA, ethylenediaminetetraacetic acid; GAPDH, glyceraldehyde 3-phosphate dehydrogenase; FACS, fluorescence-activated cell sorting; FITC, fluorescein isothiocyanate; PBS, phosphate buffered saline; HUVEC, human umbilical vein endothelial cells; HDF, human dermal skin fibroblasts; EMT, epithelial-mesenchymal transition; TGF, transform grown factor; pi, post injection

■ REFERENCES

(1) *Challenges and Opportunities Report*; U.S. Department of Health and Human Services, Food and Drug Administration: Silver Spring, MD, March 2004; http://www.fda.gov/ScienceResearch/SpecialTopics/CriticalPathInitiative/CriticalPathOpportunitiesReports-/ucm077262.htm.

(2) (a) *Backgrounder: How New Drugs Move Through the Development and Approval Process*; Tufts Center for the Study of Drug Development: Boston, November 1, **2001**; (b) Gilbert, J.; Henske, P.; Singh, A. Rebuilding Big Pharma's Business Model. *The Business & Medicine Report, Windhover Information*, November 2003; Vol. *21*, no. 10, http://www.bain.com/Images/rebuilding_big_pharma.pdf.

(3) *Innovative drug development approaches-project. Final report from THEEMEA/CHMP-THINK-TANK group on innovative drug development*; *EMEA* 2007; pp 1−26, http://www.ema.europa.eu/docs/en_GB/document_library/Other/2009/10/WC500004913.pdf.

(4) Gilbert, M. R.; Kuhn, J.; Lamborn, K. R.; Lieberman, F.; Wen, P. Y.; Mehta, M.; Cloughesy, T.; Lassman, A. B.; Deangelis, L. M.; Chang, S.; Prados, M. Cilengitide in patients with recurrent glioblastoma: the results of NABTC 03−02, a phase II trial with measures of treatment delivery. *J. Neurooncol.* **2012**, *106*, 147−153.
(5) *Cilengitide, Temozolomide, and Radiation Therapy in Treating Patients With Newly Diagnosed Glioblastoma and Methylated Gene Promoter Status (CENTRIC)*; National Institutes of Health: Bethesda, MD; http://clinicaltrials.gov/ct2/show/NCT00689221, http://clinicaltrials.gov/ct2/show/NCT00085254.
(6) For reviews see: (a) Arnaout, M. A.; Mahalingam, B.; Xiong, J. P. Integrin structure, allostery, andbidirectional signaling. *Annu Rev. Cell Dev. Biol.* **2005**, *21*, 381−410. (b) Cabodi, S.; del Pilar Camacho-Leal, M.; Di Stefano, P.; Defilippi, P. Integrin signalling adaptors: not only figurants in the cancer story. *Nature Rev. Cancer* **2010**, *10*, 858−870. (c) Shattil, S. J.; Kim, C.; Ginsberg, M. H. The final steps of integrin activation: the end game. *Nature Rev. Mol. Cell Biol.* **2010**, *11*, 288−300. (d) Desgrosellier, J. S.; Cheresh, D. A. Integrins in cancer: biological implications and therapeutic opportunities. *Nature Rev. Cancer* **2010**, *10*, 9−22. (e) Hanahan, D.; Weinberg, R. A. Hallmarks of cancer: the next generation. *Cell* **2011**, *144*, 646−674.
(7) (a) Albelda, S. M.; Mette, S. A.; Elder, D. E.; Stewart, R.; Damjanovich, L.; Herlyn, M.; Buck, C. A. Integrin distribution in malignant melanoma: association of the beta 3 subunit with tumor progression. *Cancer Res.* **1990**, *50*, 6757−6764. (b) Seftor, R. E. Role of the beta3 integrin subunit in human primary melanoma progression: multifunctional activities associated with alpha(v)beta3 integrin expression. *Am. J. Pathol.* **1998**, *153*, 1347−1351. (c) Van Belle, P. A.; Elenitsas, R.; Satyamoorthy, K.; Wolfe, J. T.; Guerry, D., IV; Schuchter, L.; Van Belle, T. J.; Albelda, S.; Tahin, P.; Herlyn, M.; Elder, D. E. Progression-related expression of beta3 integrin in melanomas and nevi. *Hum. Pathol.* **1999**, *30*, 562−567. (d) McGary, E. C.; Lev, D. C.; Bar-Eli, M. Cellular adhesion pathways and metastatic potential of human melanoma. *Cancer Biol. Ther.* **2002**, *1*, 459−465.
(8) (a) Brooks, P. C.; Strömblad, S.; Sanders, L. C.; von Schalscha, T, L.; Aimes, R. T.; Stetler-Stevenson, W. G.; Quigley, J. P.; Cheresh, D. A. Localization of matrix metalloproteinase MMP-2 to the surface of invasive cells by interaction with integrin alpha v beta 3. *Cell* **1996**, *85*, 683−693. (b) Hofmann, U. B.; Westphal, J. R.; Waas, E. T.; Becker, J. C.; Ruiter, D. J.; van Muijen, G. N. Coexpression of integrin alpha(v)beta3 and matrix metalloproteinase-2 (MMP-2) coincides with MMP-2 activation: correlation with melanoma progression. *J. Invest. Dermatol.* **2000**, *115*, 625−632.
(9) Gálvez, B. G.; Matías-Román, S.; Yáñez-Mó, M.; Sánchez-Madrid, F.; Arroyo, A. G. ECM regulates MT1-MMP localization with beta1 or alphavbeta3 integrins at distinct cell compartments modulating its internalization and activity on human endothelial cells. *J. Cell Biol.* **2002**, *159*, 509−521.
(10) Alonso, S. R.; Tracey, L.; Ortiz, P.; Pérez-Gómez, B.; Palacios, J.; Pollán, M.; Linares, J.; Serrano, S.; Sáez-Castillo, A. I.; Sánchez, L.; Pajares, R.; Sánchez-Aguilera, A.; Artiga, M. J.; Piris, M. A.; Rodríguez-Peralto, J. L. A high-throughput study in melanoma identifies epithelial−mesenchymal transition as a major determinant of metastasis. *Cancer Res.* **2007**, *67*, 3450−3460.
(11) Hynes, R. O. A reevaluation of integrins as regulators of angiogenesis. *Nature Med.* **2002**, *8*, 918−921.
(12) (a) Haubner, R.; Finsinger, D.; Kessler, H. Stereoisomeric peptide libraries and peptidomimetics for designing selective inhibitors of the alpha(V)beta(3) integrin for a new cancer therapy. *Angew. Chem., Int. Ed. Engl.* **1997**, *36*, 1374−1389. (b) MacDonald, T. J.; Taga, T.; Shimada, H.; Tabrizi, P.; Zlokovic, B. V.; Cheresh, D. A.; Laug, W. E. Preferential susceptibility of brain tumors to the antiangiogenic effects of an alpha(v) integrin antagonist. *Neurosurgery* **2001**, *48*, 151−157. (c) Kumar, C. C.; Malkowski, M.; Yin, Z.; Tanghetti, E.; Yaremko, B.; Nechuta, T.; Varner, J.; Liu, M.; Smith, E. M.; Neustadt, B.; Presta, M.; Armstrong, L. Inhibition of angiogenesis and tumor growth by SCH221153, a dual alpha(v)beta3 and alpha(v)beta5 integrinreceptor antagonist. *Cancer Res.* **2001**, *61*, 2232−2238. (d) Burke, P. A.; De Nardo, S. J.; Miers, L. A.; Lamborn, K. L.; Matzku, S.; De Nardo, G. L. Cilengitide Targeting of a_vb_3 Integrin Receptor Synergizes with Radioimmunotherapy to Increase Efficacy and Apoptosis in Breast Cancer Xenografts. *Cancer Res.* **2002**, *62*, 4263−4272. (e) Belvisi, L.; Riccioni, T.; Marcellini, M.; Vesci, L.; Chiarucci, I.; Efrati, D.; Potenza, D.; Scolastico, C.; Manzoni, L.; Lombardo, K.; Stasi, M. A.; Orlandi, A.; Ciucci, A.; Nico, B.; Ribatti, D.; Giannini, G.; Presta, M.; Carminati, P.; Pisano, C. Biological and molecular properties of a new alpha(v)beta3/alpha(v)-beta5 integrin antagonist. *Mol. Cancer Ther.* **2005**, *4*, 1670−1680. (f) Clezardin, P.; Teti, A. Bone metastasis: pathogenesis and therapeutic implications. *Clin. Exp. Metastasis.* **2007**, *24*, 599−608. (g) Trabocchi, A.; Menchi, G.; Cini, N.; Bianchini, F.; Raspanti, S.; Bottoncetti, A.; Pupi, A.; Calorini, L.; Guarna, A. Click-chemistry-derived triazole ligands of arginine-glycine-aspartate (RGD) integrins with a broad capacity to inhibit adhesion of melanoma cells and both in vitro and in vivo angiogenesis. *J. Med. Chem.* **2010**, *53*, 7119−7128. (h) Gentilucci, L.; Cardillo, G.; Spampinato, S.; Tolomelli, A.; Squassabia, F.; De Marco, R.; Bedini, A.; Baiula, M.; Belvisi, L.; Civera, M. Antiangiogenic effect of dual/selective alpha(5)beta(1)/alpha(v)-beta(3) integrin antagonists designed on partiallymodified retro-inverso cyclotetrapeptide mimetics. *J. Med. Chem.* **2010**, *53*, 106−118.
(13) For reviews, see: (a) Liu, S. Radiolabeled Multimeric Cyclic RGD Peptides as Integrin $\alpha_v\beta_3$ Targeted Radiotracers for Tumor Imaging. *Mol. Pharmaceutics* **2006**, *3*, 472−486. (b) Beer, A. J.; Schwaiger, M. Imaging of integrin $\alpha v\beta 3$ expression. *Cancer Metastasis Rev.* **2008**, *27*, 631−644. (c) Haubner, R.; Decristoforo, C. Radiolabelled RGD peptides and peptidomimetics for tumor targeting. *Front Biosci.* **2009**, *14*, 872−886. (d) Liu, L. Radiolabeled Cyclic RGD Peptides as Integrin $\alpha_v\beta_3$-Targeted Radiotracers: Maximizing Binding Affinity via Bivalency. *Bioconjugate Chem.* **2009**, *20*, 2199−2213. (f) Beer, A. J.; Kessler, H.; Wester, H. J.; Schwaiger, M. PET Imaging of Integrin $\alpha_v\beta_3$ Expression. *Theranostic* **2011**, *1*, 48−57.
(14) (a) Dijkgraaf, I.; Beer, A. J.; Wester, H. J. Application of RGD-containing peptides as imaging probes for alphavbeta3 expression. *Front Biosci.* **2009**, *14*, 887−899. (b) Schottelius, M.; Laufer, B.; Kessler, H.; Wester, H. J. Ligands for Mapping $\alpha_v\beta_3$-Integrin Expression in Vivo. *Acc. Chem. Res.* **2009**, *42*, 969−980. (c) Li, Z. B; Chen, X. MicroPET, MicroSPECT, and NIR Fluorescence Imaging of Biomolecules in Vivo. *Methods Mol. Biol.* **2009**, *544*, 461−481. (d) Zhou, Y.; Chakraborty, S.; Liu, S. Radiolabeled Cyclic RGD Peptides as Radiotracers for Imaging Tumors and Thrombosis by SPECT. *Theranostic* **2011**, *1*, 58−62.
(15) Cini, N.; Trabocchi, A.; Menchi, G.; Bottoncetti, A.; Raspanti, S.; Pupi, A.; Guarna, A. Morpholine-based RGD-cyclopentapeptides as alphavbeta3/alphavbeta5 integrin ligands: role of configuration towards receptor binding affinity. *Bioorg. Med. Chem.* **2009**, *17*, 1542−1549.
(16) Xiong, J. P.; Stehle, T.; Zhang, R.; Joachimiak, A.; Frech, M.; Goodman, S. L.; Arnaout, M. A. Crystal Structure of the extracellular domain of integrin alphaV beta3 in complex with an Arg-Gly-Asp ligand. *Science* **2002**, *296*, 151−155.
(17) Morris, G. M.; Goodsell, D. S.; Halliday, R. S.; Huey, R.; Hart, W. E.; Belew, R. K.; Olson, A. J. Automated docking using Lamarckian genetic algorithm and an empirical binding free energy function. *J. Comput. Chem.* **1998**, *19*, 1639−1662.
(18) We assumed 3′-iodo-D-Tyr side chain not to influence the conformational preferences of the cyclopeptide backbone, as confirmed by conformational analysis by molecular mechanics resulting in a similar geometry as for **1**, possessing the cis-amide bond between D-Tyr and D-morpholine-3-carboxylic acid.
(19) (a) Benaron, D. A. The future of cancer imaging. *Cancer Metastasis Rev.* **2002**, *21*, 45−78. (b) Beer, A. J.; Schwaiger, M. Imaging of integrin alphavbeta3 expression. *Cancer Metastasis Rev.* **2008**, *27*, 631−644.
(20) Christofori, G. New signals from the invasive front. *Nature* **2006**, *441*, 444−450.
(21) Laurens, N.; Engelse, M. A.; Jungerius, C.; Lowik, C. W.; van Hinsbergh, V. W.; Koolwijk, P. Single and combined effects of a_vb_3 and

a_5b_1 integrins on capillary tube formationin a human fibrinous matrix. *Angiogenesis* **2009**, *12*, 275−285.
(22) Witz, I. P. Tumor-microenvironment interactions: dangerous liaisons. *Adv. Cancer Res.* **2008**, *100*, 203−229.
(23) Kalluri, R.; Zeisberg, M. Fibroblasts in cancer. *Nature Rev. Cancer* **2006**, *6*, 392−401.
(24) Kumar, C. C.; Nie, H.; Armstrong, L.; Zhang, R.; Vijay-Kumar, S.; Tsarbopoulos, A. Chloramine T-induced structural and biochemical changes in echistatin. *FEBS Lett.* **1998**, *429*, 239−248.
(25) Gillet, A.; Sanner, M.; Stoffler, D.; Olson, A. Tangible Interfaces for Structural Molecular Biology. *Structure* **2005**, *13*, 483−491.
(26) DeLano, W. L. *The PyMOL Molecular Graphics System*; DeLano Scientific LLC: San Carlos, CA; [http://www.pymol.org].